RESEARCH ARTICLE

Macromolecular Materials and Engineering
Open Access
www.mame-journal.de

Localised Therapies Using 3D-Printed Collagen-Based Micro-Implant for Ocular Indications

Hamid Heidari Kashkooli, Arian Farokh, Sajad Mohammadi, Martina Marcotulli, Silvia Franco, Roberta Angelini, Giancarlo Ruocco, Hanieh Khalili, and Gianluca Cidonio**

Current limitations in treating retinal diseases like age-related macular degeneration (AMD) and diabetic retinopathy (DR) are due to the short ocular residence time of biologics and the difficulty of precise drug delivery. In turn, frequent injections are required, hindering patient compliance, and increasing healthcare costs. This study explores the development of a collagen-based implant using 3D bioprinting platform to address these challenges. The implant offers dual functionalities: i) sustained and localized drug delivery using in situ polymerization collagen (IPC) to act as reservoirs for prolonged release of biologics to the target tissue and ii) scaffold stability through the incorporation of methacrylated hyaluronic acid (HAMA) to enhance the mechanical properties of the IPC implant, making it suitable for 3D printing of targeted drug delivery systems. This data demonstrates that IPC-HAMA implants exhibit slow drug release and scaffold stability for over 80 days. Additionally, 3D bioprinting enables precise targeting and volumetric control within the simulated vitreous humor, overcoming challenges associated with traditional injection methods. This innovative approach has the potential to revolutionize drug delivery and localized tissue therapy for retinal diseases.

1. Introduction

Tissue and organ localized treatments are sought for a wide range of conditions. Diseases affecting the retina, such as age-related macular degeneration (AMD) and diabetic retinopathy (DR), are particularly devastating as they cause irreversible damage to essential retinal cells, leading to blindness.[1] Ocular pathologies present unique challenges due to the complex physiological barriers protecting the diseased area of the eye.[2] While intravitreal injections of biologics targeting vascular endothelial growth factor (VEGF) are the mainstay for early-stage treatment, their short ocular residence time necessitates frequent injections, fails to restore vision, and imposes a significant treatment burden and healthcare costs.[3,4] These challenges highlight the clinical need for innovative treatment strategies that offer targeted therapies that demonstrates both i) sustained drug delivery to prolong the ocular residence time of biologics and ii) tissue engineering to develop specialized implants capable of delivering cells to the target tissues, thereby replacing damaged retinal cells.[5,6] Our goal is to develop a collagen-based implant using 3D bioprinting method to address these challenges and provide localized therapies with dual functionalities. Central to the success of such endeavors depends on the selection of biomaterials and the methods employed for scaffold fabrication and drug delivery.[7]

H. H. Kashkooli, H. Khalili
School of Medicine and Biosciences
University of West London
London W5 5RF, UK
E-mail: hanieh.khalili@uwl.ac.uk

A. Farokh
School of Computing and Engineering
University of West London
London W5 5RF, UK

S. Mohammadi, M. Marcotulli, G. Ruocco, G. Cidonio
Center for Life Nano- & Neuro-Science (CLN2S)
Fondazione Istituto Italiano di Tecnologia
Rome 00161, Italy
E-mail: gianluca.cidonio@uniroma1.it

S. Franco, R. Angelini
Institute for Complex Systems (ISC-CNR) and Department of Physics
Sapienza University of Rome
Rome 00185, Italy

H. Khalili
School of Pharmacy
University College London
London WC1N 1AX, UK

G. Cidonio
Department of Mechanical and Aerospace Engineering
Faculty of Civil and Industrial Engineering
Sapienza University of Rome
Rome 00184, Italy

The ORCID identification number(s) for the author(s) of this article can be found under https://doi.org/10.1002/mame.202400236

DOI: 10.1002/mame.202400236

Collagen emerges as a favourable candidate among naturally derived biomaterials, due to its exceptional biocompatibility, biodegradability, and ability to interact with various cell types.[8,9] Injectable hydrogel materials have shown promise in various ophthalmic applications,[10,11] leveraging their porous architecture to serve as reservoirs for drugs and/or cells, enabling controlled and localized release of biologics to target tissues,[12] while mitigating systemic exposure.[13,14] Nonetheless, the inherent high-water content and large pore dimensions of hydrogels often result in a burst of initial drug release.[15] Type I collagen is considered an optimal gel system, capable of spontaneous assembly upon neutralization and incubation at physiological temperatures (37 °C), as well as rapid fibrillogenesis.[16] To improve the stability of collagen, we proposed the incorporation of ethylenediaminetetraacetic acid (EDTA) during collagen preparation. This approach stabilizes the collagen in solution at ambient temperature allowing it to fibrillate upon exposure to physiological solutions at 37 °C.[17] The resulting collagen is termed in situ polymerization collagen (IPC),[18,19] which offers the potential for direct injection as a liquid solution into the target tissue site, which is particularly beneficial for minimally invasive procedures.[20] However, IPC application as a 3D implant is somewhat constrained by the poor mechanical properties.[21] To address this limitation, various strategies have been suggested to enhance its biomechanical properties encompassing chemical crosslinker, covalent conjugation, and polymer grafting, or blending.[22] We aimed to incorporate and crosslink collagen with either methacrylated hyaluronic acid (HAMA) or gelatin methacryloyl (GelMA) to produce either IPC-HAMA or IPC-GelMA, respectively. The inclusion of polymer content with tuneable crosslinking properties is appealing to sustain the release of encapsulated drug cargos.

Traditional injection of biological drugs for retinal diseases presents limitations. Highly trained personnel strife to localize injection volumes within the vitreous humor.[23] Furthermore, the drug delivery method is heavily influenced by the unique compositions of the vitreous humor.[24] Indeed, the vitreous humor is a clear gel-like substance between the lens and retina which plays a vital role in maintaining retinal function.[25] Although it is composed of more than 90% water, the humor also contains a network of collagen and hyaluronic acid Fibres.[26] However, the biomechanical properties of vitreous humor deteriorate with age, stimulating a cascade of events such as the decrease in viscoelastic characteristics, which in turn greatly limit drug delivery,[27,28] and increase drug reflux, impairing the targeting of specific areas for optimal treatment.[29] Alternative platforms capable of precise delivery of drugs to the eye tissues are being explored.[29] 3D bioprinting emerges as a revolutionary approach for targeted drug delivery in the eye, offering precision and accuracy by controlling injection volume, depth, and speed.[30,31] This might reduce variability and ensure consistent delivery to the desired location within the vitreous humor. The research data here reported, demonstrate the use of a 3D bioprinter to deposit different biomaterial blends (IPC and IPC-HAMA) into specific locations within a simulated vitreous humor environment (agarose-HA support bath), which in turn holds the potential to revolutionize the field of drug delivery and localized tissue therapy.

2. Results and Discussions

Ocular delivery of therapeutic biologics is still challenging due to the poor site retention as well as the precision in drug/volume delivery. Herein, we present a novel approach based on the use of a custom-made 3D bioprinter extrusion system for the rapid, precise, and consistent injection of discrete volumes of drug-filled biomaterials within a vitreous simulant platform.

2.1. Collagen-based Biomaterials can be prepared to Augment Collagen Properties

The preparation of collagen-based biomaterials begins with the generation of in situ polymerizing collagen (IPC). This first step involves concentrating the collagen type I. Initially, collagen type I was precipitated from an NaCl solution, as collagen is not fully dissolved at high concentrations (Figure S1a, Supporting Information). Dialysis was then performed against acetic acid overnight, which resulted in the formation of a clear solution within the dialysis membrane (Figure S1b, Supporting Information). To further stabilize the collagen, the dialysis solution was changed to a series of EDTA solutions with increasing pH levels (ranging from pH 5 to pH 7). This gradual increase in pH allowed EDTA to bind effectively to the collagen molecules, making them soluble and stable at pH 7. In addition, the pH adjusted EDTA solution allowed the production of colorless collagen. The use of sucrose and D-mannitol in the EDTA solution during the last step of dialysis aided in the stability of the viscous collagen.[17,18] The collagen solution was collected in a clear and transparent state, showing no signs of typical fibrillogenesis, unless it was subjected to physiological stimuli (Figure S1c, Supporting Information).

The fibrillation process of IPC occurred in a relatively short time (5 min) after incubating with an aqueous PBS buffer at a temperature of 37 °C. This caused the solution to transform from a clear viscous state to an opaque, solid gel (**Figure 1**a). The presence of EDTA within the IPC formulation was crucial, as it was introduced during dialysis to prevent spontaneous polymerization. When exposed to heat and PBS buffer, the displacement of EDTA molecules prompted the formation of banded collagen fibrils. Using a hydroxyproline assay, the concentration of IPC was determined to be 23.72 mg mL^{-1} ($\pm$1.99 mg mL^{-1}, 12.5 mL). This corresponds to a recovery yield of 99%, starting from 300 mg collagen type I and producing 296.5 mg IPC. The injectability of the IPC gel was evaluated using different syringe sizes (22, 27, and 29 G). The gel was injectable with minimal pressure and did not produce bubbles in any syringe size, even with the finest needle (25 or 29 G) (Figure 1b). However, 3D printing with IPC gel alone resulted in scaffolds with insufficient mechanical strength for stability. This was evident when depositing a canonical mesh-like, 3D structure (Figure 1c). Scaffolds printed into the support bath did not maintain their 3D properties after the fibrilization process for more than 24 h (Figure 1d).

To address the limitations of IPC gel's mechanical strength for 3D printing, we investigated blending it with biocompatible materials, like hyaluronic acid (HA) or gelatin. Particularly, methacrylated HA, or HAMA emerged as a promising candidate for IPC support due to the tuneable viscosity and crosslinking potential.[32] We hypothesized that blending HAMA

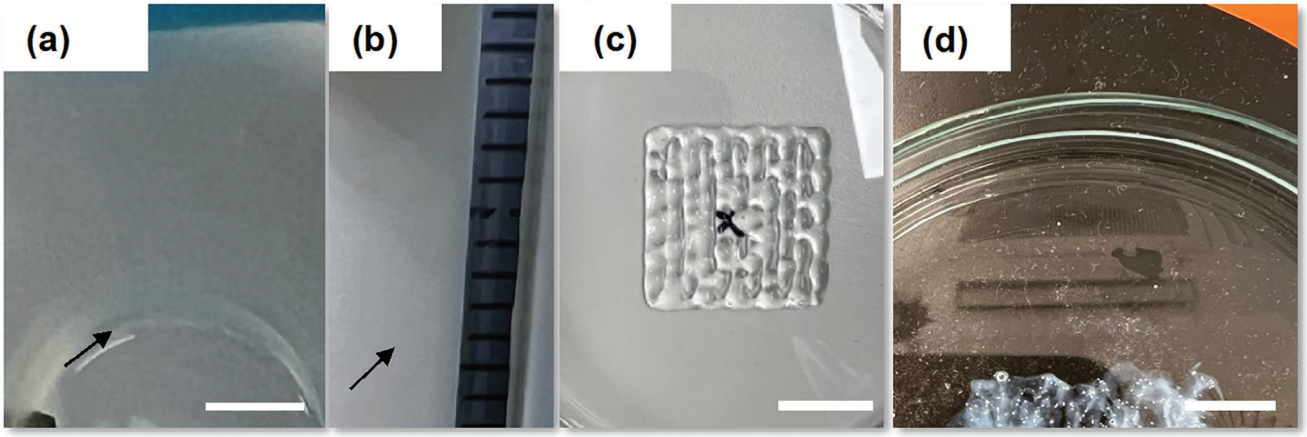

Figure 1. Images showing the IPC fibrilization, injectability and 3D printability, a) IPC fibrilization in PBS at 37 °C within 5–10 min, b) Injectability using needle sizes 22 to 29 G without bubble formation, c) IPC-alone, 3D printed into the air, structure of scaffold collapsed due to weak mechanical strength and d) Loss of 3D shape when IPC alone 3D printed into support bath, within 24 h. Scale bar (a,c,d) 3 mm.

or GelMA (methacrylated gelatin) with IPC could achieve a trifecta of benefits: i) enhanced printability, ii) improved mechanical strength for stable 3D structures, and iii) prolonged drug release. This composite material could then hold potential for applications like micro-implants capable of sustained drug release.

2.2. HAMA and GelMa Synthesis and Analysis

HAMA was synthesized by covalently modifying HA with methacrylate groups. This modification targeted the carboxylic acid groups in the HA structure, which were activated using EDC, a common carbodiimide. EDC facilitated the formation of reactive O-acylisourea intermediates, capable of reacting with amines to create amide bonds.[33] To enhance the stability of these intermediates, NHS was added, forming stable NHS esters and reducing the risk of premature hydrolysis, thereby improving the efficiency of the subsequent reaction with AEMA. In the FTIR spectra of the product, all the fingerprint peaks of HA (Figure S2a, Supporting Information) are demonstrated in the FTIR spectra of HAMA, with peaks relevant to the content of HA (Figure S3a, Supporting Information). The peaks ≈1377 and 1410 cm^{-1} could be respectively assigned to CH_3 and C–O stretching vibrations in the carboxylate group (COO–), both of which are part of the methacrylate moiety.

In the ^{1}H-NMR spectra (Figure S2b, Supporting Information), the sugar rings in hyaluronic acid can be seen between 3 and 4.5 ppm, along with two peaks ≈6 ppm, representing the methacrylation (Figure S3b, Supporting Information), which was 14%. Additionally, the sharp peak at 5.8 ppm is attributed to the self-reacted EDC. As reported, using EDC/NHS may lead to producing side products.[34,35] The initially formed active O-acylisourea groups may react not only with primary amines and NHS but also with EDC and water. The side reaction of O-acylisourea with water results in hydrolysis, reducing the efficacy of EDC. To address this, after synthesis, the HAMA was extensively dialyzed with DI water to remove any residual EDC/NHS or impurities, ensuring a pure product suitable for crosslinking and radical polymerization.[33,36] GelMA synthesis typically involves reacting methacrylic anhydride (MA) with gelatin, but a byproduct, methacrylic acid, lowers pH and hinders the reaction. To overcome this, researchers have used methods like sequential MA addition with pH control, as demonstrated by Lee et al.[37] and in this study using PBS with pH 7.4. This maintains favorable reaction conditions, promoting greater functionalization and minimizing byproducts.

As evidenced in the FTIR spectra (Figure S3c, Supporting Information), identical peaks to those observed in gelatin were noted in GelMA. At 1032 cm^{-1}, C–N stretching absorption could mean that the NH2 groups in gelatine have been changed to NH–R, meaning that the methacrylation has been successfully performed. In the ^{1}H-NMR spectra (Figure S3d, Supporting Information), the fingerprints of gelatin can be seen, along with two peaks ≈6 ppm, representing the methacrylation.

2.3. Biomechanical Characterisation of Collagen-based Biomaterials

To assess the mechanical properties of hydrogels before 3D printing, the IPC-based scaffolds were created by blending with either GelMA or HAMA using simple syringe-syringe mixing methods (**Figure 2**). Cylindrical scaffolds with a volume of 70 µL were then cast into molds and subjected to 405 nm light to initiate crosslinking. As the transparent PDMS molds permitted light penetration, the photocrosslinking process stabilized the IPC-HAMA or IPC-GelMA structure. By forming gels with a 1:2 volume ratio of IPC to HAMA or GelMA, the optimal gelation was achieved. This method produced structurally robust scaffolds, easily removable from the molds, which were then immersed in PBS buffer solutions to facilitate further fibrillation. The schematic illustration of the interaction between HAMA or GelMA with IPC is shown in **Figure 3**. Ru/SPS, acting as a photoinitiator, generated free radicals upon light exposure in HAMA (or GelMA). These free radicals initiated the polymerization of HAMA (or GelMA), leading to the formation of a crosslinked hydrogel network. While IPC can self-assemble into fibrils under physiological conditions to form

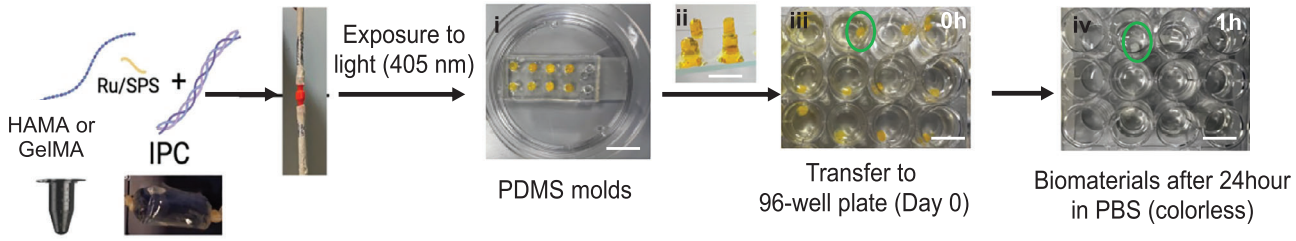

Figure 2. Representative preparation of IPC-blends biomaterials using PDMS molds, IPC-blend is colorless after being incubated in PBS for 24 h. Scale bar i) 30 mm, ii) 1 mm, iii, iv) 10 mm.

a basic collagen network,[17] it can interact with the reactive sites on HAMA (or GelMA) through its functional groups (primary amine and hydroxyl groups).[38] The primary amine on IPC can then react with these sites, forming covalent linkages that further enhance the mechanical properties of the hydrogel. Additionally, Ru(III) species might oxidize tyrosine residues in collagen, generating tyrosyl radicals that may crosslink with methacrylate radicals or other collagen molecules.[38–40] After 24 h, the photoinitiator diffused out of the scaffolds, rendering them colorless gels. These resulting gels, with their crosslinked networks, exhibited sufficient mechanical strength for subsequent experimentation. Notably, visible light-based Ru/SPS photo-initiators offer accelerated polymerization and enhanced penetration, allowing uniform curing in deeper layers. Importantly, the Ru/SPS system has demonstrated low cytotoxicity and high biocompatibility for ocular applications.[38,41,42]

2.4. Swelling and Degradation tests for Collagen-based Biomaterial

The swelling, degradation rate, and stability of IPC-based biomaterials casted in the cylindrical molds were investigated.

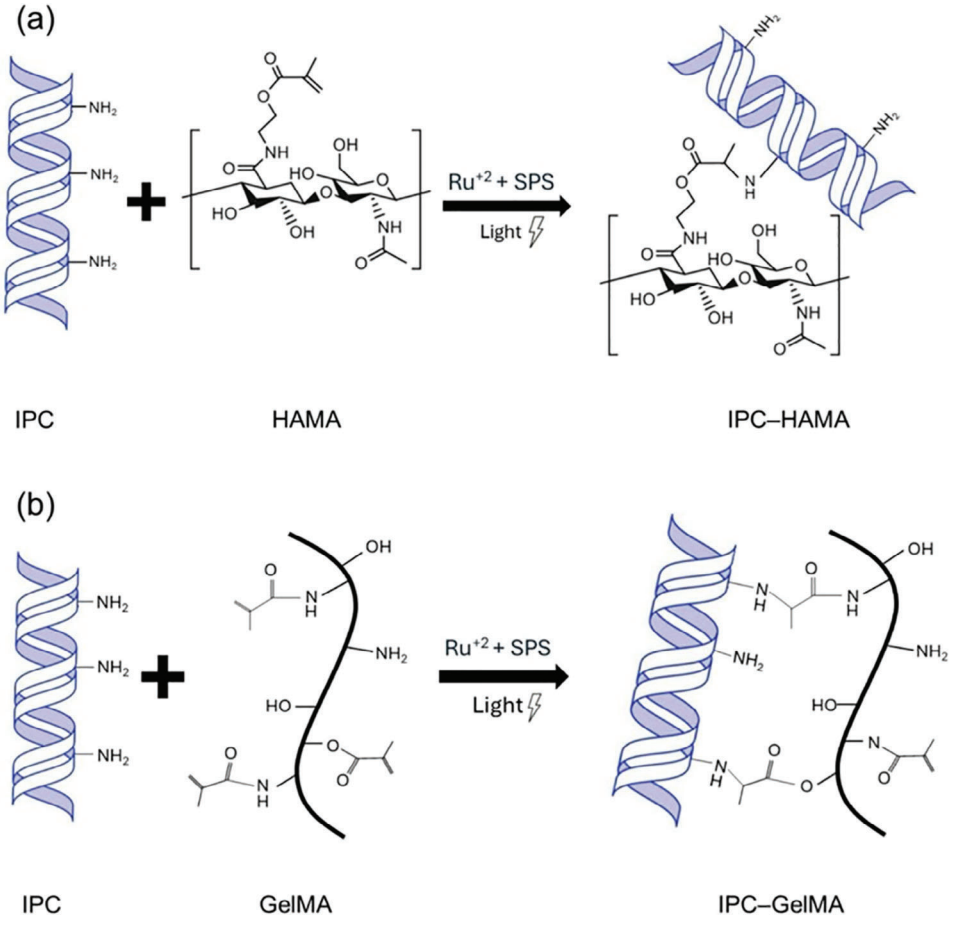

Figure 3. Schematic representation of the reaction mechanism for a) IPC–HAMA, and b) IPC–GelMA favored by the photocrosslinking mechanisms exploited to ultimately crosslink the composites.

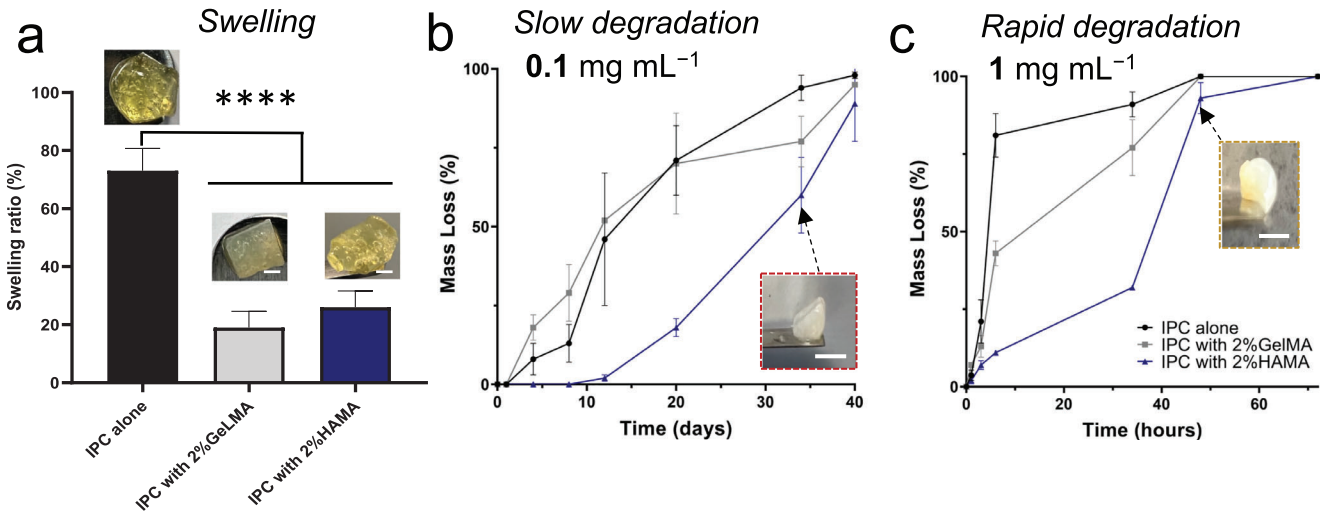

Figure 4. Investigating simulated swelling and degradation of IPC. (Moulds fabricated by IPC-composites casting were crosslinked with visible light and with temperature transition at 37 °C). Swelling a) can be controlled by the inclusion of polymeric fillers. Collagen-based hydrogels experienced b) slow enzymatic degradation at a collagenase concentration 0.1 mg mL^{-1} and c) rapid enzymatic degradation at 1.0 mg mL^{-1}. Mean ± SD, n = 3, **** $p <$ 0.0001. Scale bar (a, b, c) 1 mm.

The fabricated biomaterials were observed to swell over time, ultimately achieving a significantly lower percentage of volume change compared to IPC alone (**Figure** 4a). The drastic alteration of the swelling ability is due to the electrostatic interaction between IPC and HAMA or GelMA, resulting in a more stable assembly for printing or injection. The meshes were then exposed to low (0.1 mg mL^{-1}, Figure 4b) and high (1.0 mg mL^{-1}, Figure 4c) concentrations of collagenase enzyme to emulate slow or fast degradation within a simulated in vivo scenario, respectively. IPC alone displayed rapid degradation, losing mass in less than 10 h when exposed to a high enzyme concentration. Blending IPC with either HAMA or GelMA significantly slowed this degradation, with HAMA demonstrating the most remarkable effect by stabilizing the material for over 70 h. Interestingly, although the high enzyme concentration caused faster degradation in IPC and IPC-GelMA, the HAMA composite remained stable even after 40 days when using low enzyme concentration.

2.5. Physical Characterisation of Collagen-based Biomaterial

Scanning Electron Microscopy (SEM) is a valuable tool for visualizing the surface morphology, texture and presence of pores and Fibres in the biomaterials. In addition, pore size distribution can be measured using SEM images. We used environmental SEM (ESEM), which allows for the observation of samples in their native, hydrated gel state. This is particularly advantageous for studying biomaterials, as it eliminates the need for harsh drying processes that can alter the sample's morphology and properties. Using ESEM enabled us to visualize the formation of collagen fibrils in the IPC after being fibrilized at 37 °C and overall organization within the scaffold.

ESEM images of the IPC blends (**Figure** 5a) revealed distinct morphological differences before (i-ii) and after collagen (iii-iv) fibrilization. The collagen fibers formed in the IPC-HAMA exhibited a more homogeneous and well-organized fibrillar network compared to the IPC-GelMA and IPC alone. This suggests that HAMA might promote a more efficient fibrilization process with the IPC matrix. When observed under ESEM after being 3D printed and cross-linked (Figure 5b), the IPC-HAMA scaffold exhibited both interconnected pores and well-organized collagen fibers. This interconnected network of pores and fibers suggests the potential of this biomaterial to serve as a scaffold for cell attachment, proliferation, and potentially for sustained drug release within the pores. However, it is important to note that ESEM is primarily a qualitative imaging technique and provides limited quantitative information about the material's properties. Further work is necessary to fully characterize the mechanical properties of the IPC biomaterials using a rheometer.

2.6. Rheological Characteristics of IPC Blends

The rheological characterization revealed the temperature-dependent viscosity for IPC biomaterial with greater viscosity at 25 °C (**Figure** 6a) compared to 37 °C (Figure 6b). Both IPC and its blended biomaterials exhibited shear-thinning behavior, characterized by a decrease in viscosity as the applied shear rate increases. This non-Newtonian behavior is typical of solutions containing long, entangled molecules. High shear forces disrupt the molecular interactions, leading to a decrease in viscosity. Consequently, this shear-thinning behavior renders them impractical for direct 3D printing in the air due to insufficient viscosity to maintain structural integrity during the printing process. Interestingly, IPC blended with HAMA or GelMA was found to be less affected by temperature and characterized by the formation of a Newtonian plateau at low and high shear rates (Figure 6b). This observation suggested that the addition of HAMA or GelMA to IPC modified its rheological properties, potentially due to interactions between the components that alter the molecular conformation and entanglement within the blend.

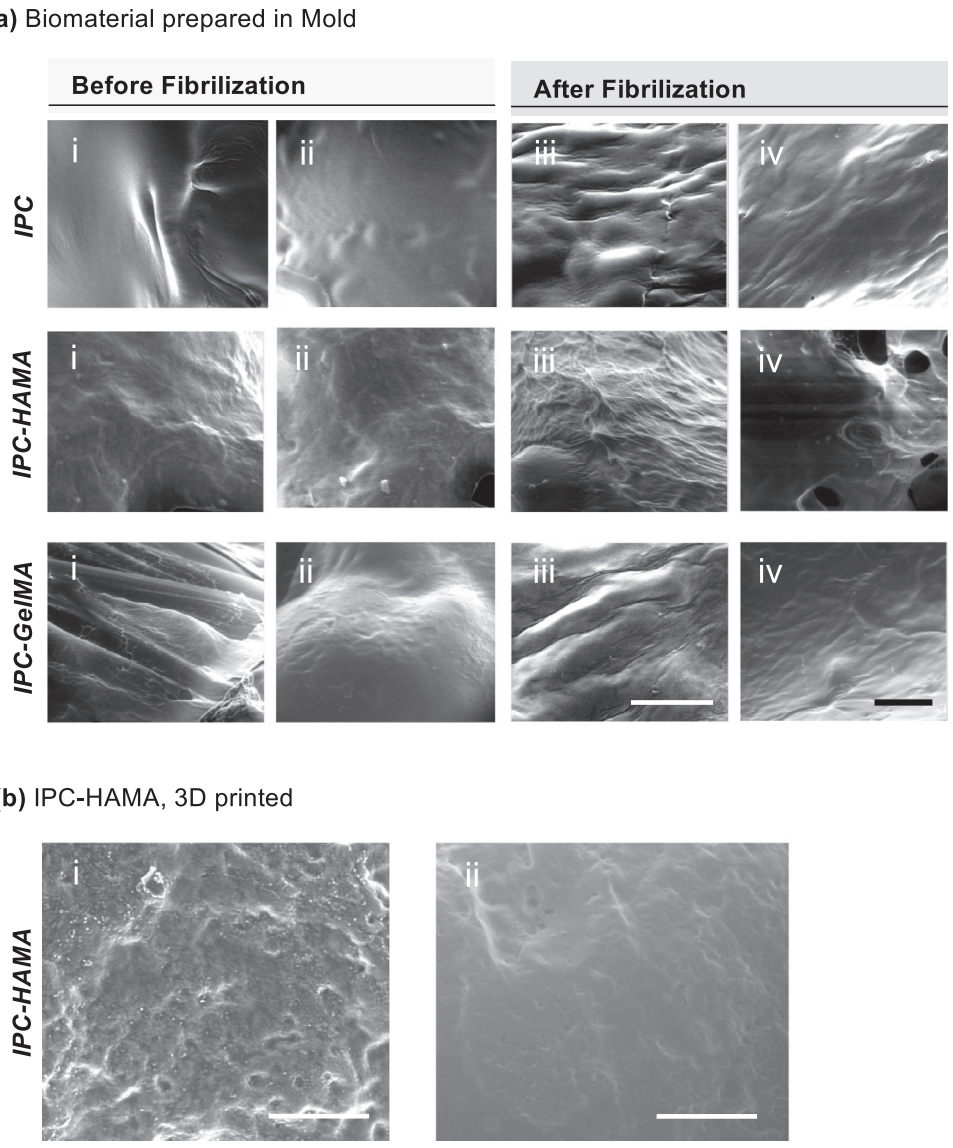

Figure 5. a) ESEM of biomaterials generated by molds, IPC, IPC-HAMA, and IPC-GelMA before and after collagen fibrilization (without Ru/SPS for cross-linking). b) ESEM of IPC-HAMA after being 3D printed and cross-linked as a scaffold. Scale bars: a – (i, iii) 300 µm, (ii, iv) 1 mm; b – 200 µm.

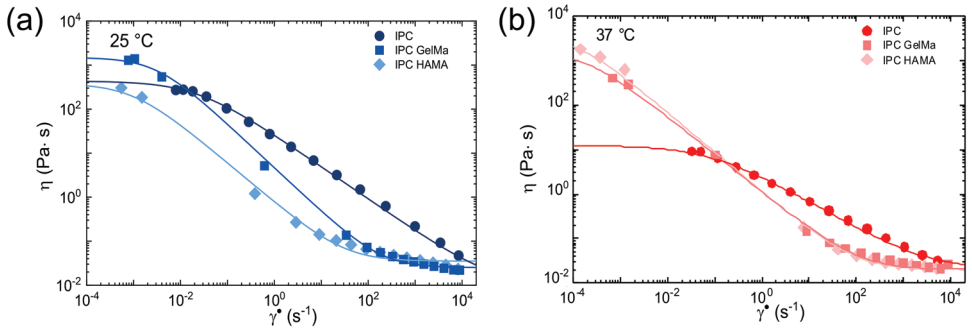

Figure 6. Rheological analysis of IPC-based composites. Investigation of viscosity at a) 25 and b) 37 °C. IPC-HAMA and IPC-GelMA demonstrated higher viscosity and improved shear-thinning behavior compared to IPC at 37 °C.

2.7. 3D Printing of the Collagen-based Biomaterials

Ideal scaffolds require biocompatibility, and biodegradability for successful tissue integration.[43] They should be designed to mimic surrounding ECM and to fit the targeted tissue, including its mechanical properties.[44] While we are investigating the biomechanical properties of IPC blends, we also recognize the importance of a fabrication process that can produce scaffolds with diverse architectures and dimensions that align with the specific requirements of the target tissue. Using a 3D printer with a 25-gauge needle and a printing speed of 160 mm min^{-1}, we were able to fabricate cylindrical IPC-HAMA implants with a diameter of 3 mm and a length of 10 mm (Figure S4a, Supporting Information). These implants maintained their distinct layers over time, as shown in Figure S4b, Supporting Information, demonstrating good structural integrity. The photoinitiators (Ru/SPS) used at a safe, low concentration (1:10 ratio) rapidly diffused outside the main printed structure, as previously reported.[38,45]

Our aim is to develop a micro-implant for retinal regeneration. The retina tissue is located at the back of the eye, in close proximity to the human vitreous. Thus, the implant can be deposited into the vitreous, which has unique mechanical and rheological properties. Therefore, we designed the support bath not only to maintain the 3D structure of the scaffold during and after the printing process but also to mimic the properties of the human vitreous. The viscosity of the prepared support baths is shown in Figures S4 and S5, Supporting Information. Viscosity as a function of shear rate is shown in Figure S5, Supporting Information for both agarose and agarose-HA fluid-gel supports. A clear shear thinning behavior is observed for both samples with low viscosity values for agarose-HA, pointing out that the addition of HA tends to fluidize the sample. Figure S6, Supporting Information highlights the transition from solid-like ($G' > G''$) to fluid-like ($G' < G''$) behavior of both fluid-gel systems. This transition is nearly reversible with essentially similar solid-like and fluid-like behavior under low and high shear strains for agarose as the sample is subjected to different cycles of low and high strain. The values of the dynamical moduli almost recovered when deformation is removed ($\gamma = 0$, white regions). On the contrary, agarose-HA does not recover completely its initial state, possibly due to the disruptive interaction of agarose with HA polymer chains, and the lower content of agarose compared to the control fluid-gel. The unique rheological properties of the prepared vitreous humor can facilitate the biomimicry of the in vivo release of biological compounds.

2.8. Sustained Drug Release from IPC Micro-Implant

Taking into consideration the physico-chemical properties of the IPC-blends, we selected IPC-HAMA as the best candidate for drug retention and tissue repair. Thus, the studies performed for the investigation of sustained drug release and printability have been carried out using exclusively this specific blend.

To study the release profile, an effective protein detection method needed to be explored. Traditional UV–visible spectroscopy at 280 nm was not suitable for monitoring the release profile of biologics from the IPC-based scaffold due to interference from collagen, which also absorbs light at this wavelength. To achieve this, IgG was fluorescently labelled with NHS-rhodamine dye, addressing the limitation of protein quantification in UV–visible spectroscopy. NHS-Rhodamine dye to antibody molar ratio of 10 was used to achieve 3.0 degrees of labelling (DOL), which balanced detection sensitivity with minimal impact on the drug's functionality.[46–48]

To ensure the stability and purity of the labelled IgG, size exclusion chromatography (SEC) and SDS-PAGE analysis were employed (Figure S7, Supporting Information). As is shown in Figure S7a, Supporting Information, the SEC peak that appeared for labelled IgG (1.0 mg mL^{-1}) at 1.8 min was similar to the SEC peak that appeared for the standard IgG (1 mg mL^{-1}), indicating that the labelling process did not affect the drug's purity or concentration. To further confirm the stability of the labelled IgG, SDS-PAGE gels displayed one single band at about 150 kDa, consistent with the expected molecular weight of IgG. In Figure S7b, Supporting Information, lanes 3 and 4, no aggregation or dissociation of light and heavy chains was observed, and no extra bands were detected compared to the control IgG.

Lyophilized labelled-IgG (2 mg), was then mixed with IPC or IPC-HAMA (80 µL) and 3D printed into an HA-Agar support bath with a cylindrical shape (3 mm × 5 mm dimensions). For photocrosslinking, the printed meshes were exposed to the light and then transferred to a solution of PBS for fibrilization. Fluorescence-based microplate readings were used to monitor the cumulative release of biologics from these scaffolds. **Figure 7a** visually demonstrates a clear distinction in the release profiles of labelled IgG between scaffolds fabricated with IPC alone and those containing IPC-HAMA biomaterials. The IPC-only scaffolds exhibited a rapid release, with nearly all labelled IgG (pink colour) released within the first 24 h. In contrast, the presence of labelled IgG (pink colour) persisted within the IPC-HAMA scaffolds even after the more than 80 days study period, indicating prolonged drug release. Quantitative analysis in Figure 7b confirms these observations. Scaffolds fabricated solely from IPC exhibited a significant burst release, with over 72% of the loaded labelled IgG released within the initial 48 h. Conversely, IPC-HAMA scaffolds displayed a more controlled and sustained release pattern. This sustained release is statistically significant ($p < 0.05$), suggesting that the incorporation of HAMA significantly prolongs the release of the labelled IgG and reduces the initial burst effect. Notably, IPC-HAMA scaffolds were able to sustain the release of the loaded biologics, with ≈70% of the drugs released in 82 days. SDS-PAGE analysis (Figure 7c) stained with silver staining for enhanced sensitivity and detection of any trace protein, demonstrates a stable, intact band (lanes 7 and 8) ≈150 kDa for IgG released from IPC-HAMA scaffold after 28 and 52 days. Conversely, no band was observed (lanes 5 and 6) for the solution collected from IPC-alone after 2 days. The results demonstrate that IPC-HAMA scaffolds provide a more consistent and sustained release profile, ensuring the structural integrity of the scaffold and the released biologic, which is critical for achieving therapeutic goals in sustained delivery systems.

To evaluate the in-vitro degradation profile of the collagen-based scaffolds under simulated physiological conditions relevant to ocular drug delivery, a biodegradation test was conducted. Collagen-based scaffolds (IPC alone and IPC-HAMA) loaded with labelled IgG were submerged in PBS solution containing

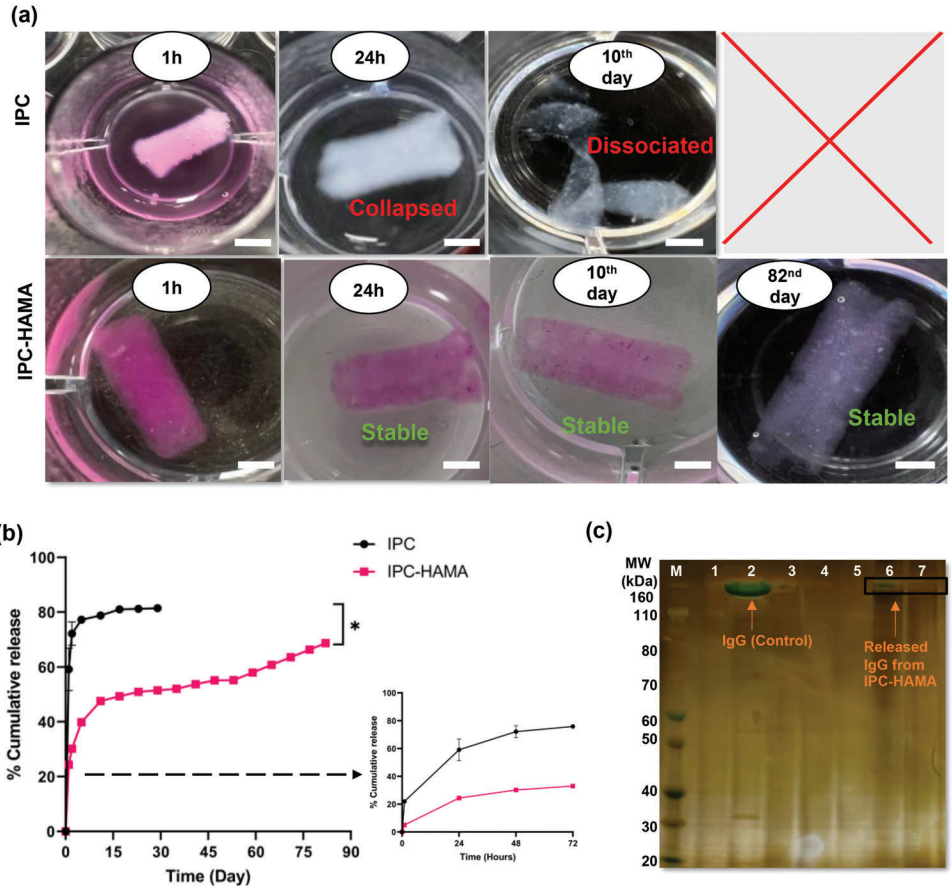

Figure 7. a) Images of 3D-printed scaffolds with labelled IgG show colour changes over time, indicating drug release in PBS buffer solution. The IPC scaffold collapsed immediately after the fibrillation process. It became colorless after 48 h, indicating a high level of drug efflux. By the tenth day, the scaffold had degraded and dissociated. In contrast, IPC-HAMA scaffolds remained intact, suggesting sustained drug retention, with viable structures up to day 82. Scale bar: 3 mm b) IgG release profile from IPC or IPC-HAMA scaffold in PBS. (*: $p < 0.05$, a significant difference between IPC scaffold and the IPC-HAMA scaffold (n = 3)). c) The Novex Bis-Tris 4–12% gels stained with silver staining; Lane 1: Protein standard. Lane 2: IgG (control). Lane 3: IgG (post-purification control). Lanes 4–6: IgG solutions collected from IPC-alone scaffold day 2, 4, and 6. Lanes 7–8: IgG solutions collected from IPC-HAMA scaffold days 28 and 52.

collagenase (0.5 mg mL^{-1}) and hyaluronidase (0.3 U mL^{-1}) for 17 days. Collagenase specifically degrades collagen, a major component of both the scaffolds and the vitreous humor, mimicking the natural enzymatic breakdown within the eye. Hyaluronidase breaks down hyaluronic acid (HA), another key component of the vitreous humor, providing a more realistic representation of the enzymatic environment. The chosen enzyme concentrations represent a balance between achieving a measurable degradation rate and maintaining relevance to physiological conditions.[49,50] Based on the presence of these enzymes in the vitreous humor, we anticipated that the scaffolds would undergo a gradual degradation process over time when exposed to the enzyme solution. Monitoring the scaffold integrity and the release of labelled IgG throughout the 17-day test provided valuable insights into their biodegradability profiles (**Figure 8**). As expected, the rate of degradation was slower for IPC-HAMA compared to IPC alone (Figure 8a). The IPC-alone scaffold was fully degraded after 7 days in enzyme solution, while IPC-HAMA scaffold remained stable until 18 days when all the IgG was released (Figure 8b).

As demonstrated in Figure 8b, the release of biologics from both IPC alone and IPC-HAMA scaffolds followed first-order release kinetics, characterized by exponential decline in the remaining drug concentration over time. The IPC-alone scaffolds, however, displayed a significant burst release when exposed to enzyme solution. ≈31% of the loaded IgG was released within the first 3 h, followed by a rapid increase to 72% release within 24 h. IPC-HAMA, in contrast, exhibited a significantly slower release profile when exposed to enzyme solution. Only 13% of the loaded biologics were released within the first 3 h, with a total of 17% released after 24 h. This delayed release suggests that the HAMA component likely contributes to increased scaffold stability, thereby reducing burst effects, and enabling an extended-release profile. By day 15, nearly 50% of the biologics had been released in an enzyme solution from the IPC-HAMA scaffold. This continued release, with 85% by day 17 when the scaffold was completely degraded. The accelerated release was statistically significant (p-value: 0.0095).

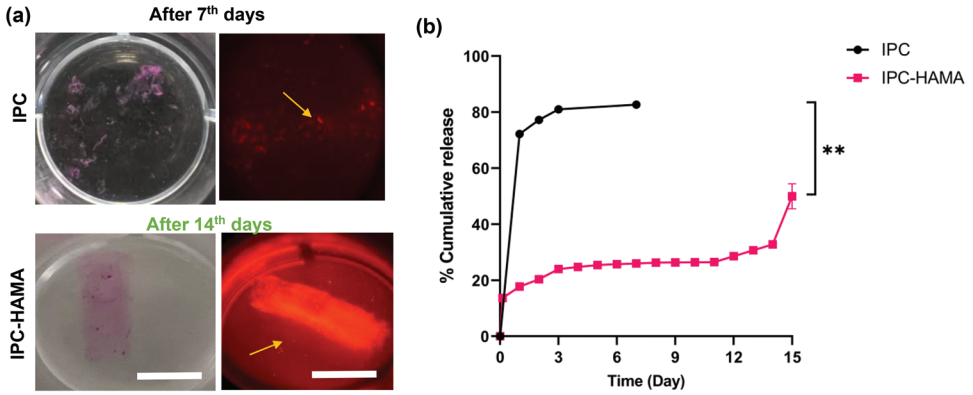

Figure 8. Biodegradation analysis of 3D collagen-based scaffolds a) Fluorescence microscopy images of labelled IgG released from scaffolds under enzymatic degradation. The red fluorescence indicates where the labelled IgG is released from the scaffolds (yellow arrow). Scale bar: 3 mm b) Release profiles of labelled IgG from IPC and IPC-HAMA scaffold stored in an enzyme solution. Data are shown as means ± SD (n = 2). Statistical significance is indicated by **($p = 0.0095$), indicating the levels of significant differences in release rates between the two scaffold types.

2.9. Localised Delivery of IPC-Biomaterials using 3D Printer

Using computer-aided design (CAD) and 3D printing, we wished to deposit the biomaterials with interconnected pores in various configurations and locations (**Figure 9a**) using different nozzle sizes (25 and 21 G) and volumes (30 and 100 µL). Rhodamine dye was added to collagen biomaterials to test the dye dispersion and how dye diffused out of the biomaterial when deposited in the HA-Agar support bath. A coloured dye was employed as a surrogate molecule to simplify the diffusion test. This approach facilitated visualization using imagining techniques, allowing for easier evaluation of drug release behavior. After 24 h, faster dye diffusion was observed in the IPC alone and IPC-GelMA compared to the IPC-HAMA biomaterials (Figure 9b). Notably, increasing the biomaterial deposition volume led to even faster dye diffusion in the IPC-GelMA, regardless of the nozzle gauge used. Interestingly, HAMA appeared to play a crucial role in preserving dye diffusion, particularly for low-volume depositions (30 µL). While both blends exhibited faster dye diffusion with a larger deposition volume (100 µL), the inclusion of HAMA resulted in significantly improved dye retention compared to controls, as shown in Figure 9c,d.

To repeat the dye diffusion test and explore how deposition location affects stability, IPC composites were incorporated with a biological drug similar in molecular size to IgG. The drug-loaded biomaterials were then deposited at various locations within a HA-Agar support bath using a 3D printer (Figure 9e,f). Initially, IPC and IPC-HAMA scaffolds exhibited promising biologic release, with ≈56% and 63% released, respectively, upon surface deposition in the support bath.

Conversely, when deposited deeper within the support bath, the IPC-HAMA biomaterials demonstrated superior stability compared to other IPC blends, although other IPC biomaterials also showed improved stability when deposited in a deep location. This observation suggests that depositing the biomaterial deeper within the vitreous humor might enhance the stability of the scaffold. Furthermore, a notable decrease in biologic release to 16% for IPC and 14% for IPC-HAMA was noted upon deep deposition in the vitreous simulant (Figure 9g), indicating a significant impact of injection depth on release kinetics, likely due to concentration gradients and diffusion dynamics. As the biomaterials absorbed water from the support bath, swelling occurred, potentially contributing to dissociation if not adequately supported. Deeper deposition within the bath might provide better containment for the swelling pressure.

Further studies are necessary to elucidate the precise mechanisms underlying the observed differences in stability based on deposition location. This preliminary data suggests that by using 3D printing and CAD, we were able to successfully deposit biomaterials at different locations within simulated ocular vitreous with varying injection volumes.

3. Conclusion

Intraocular injection remains a challenging clinical procedure, demanding highly skilled personnel and specialized equipment. Our study introduces a novel approach utilizing biomaterial-based intravitreal implants composed of IPC blends. These blends, incorporated with HAMA or GelMA, demonstrate controlled swelling, enhanced degradation resistance, and favourable rheological properties, making them ideal for 3D deposition systems such as printing and injection. By employing an agarose-HA simulant gel bath, we successfully deposited and localized IPC composites in three dimensions, showcasing the release of therapeutic compounds at various ocular depths. By driving a 3D bioprinting platform and tailoring the deposition as automated injection, we potentially ensured accurate placement and dosage for individual patients. Our research illustrates that integrating IPC with tailored biomaterials can achieve controlled and sustained drug release for up to 80 days while maintaining scaffold stability. This finding highlights the promising therapeutic potential of this approach for localized tissue therapy. Further investigation is needed to elucidate the pre-clinical functionality of this approach, further ameliorating the automation and drug delivery capabilities.

4. Experimental Section

Materials: Pepsin Soluble Collagen (6 mg mL^{-1}) in 0.01 M HCl 100 mL (cat no. FS22005), purchased from Collagen solutions.

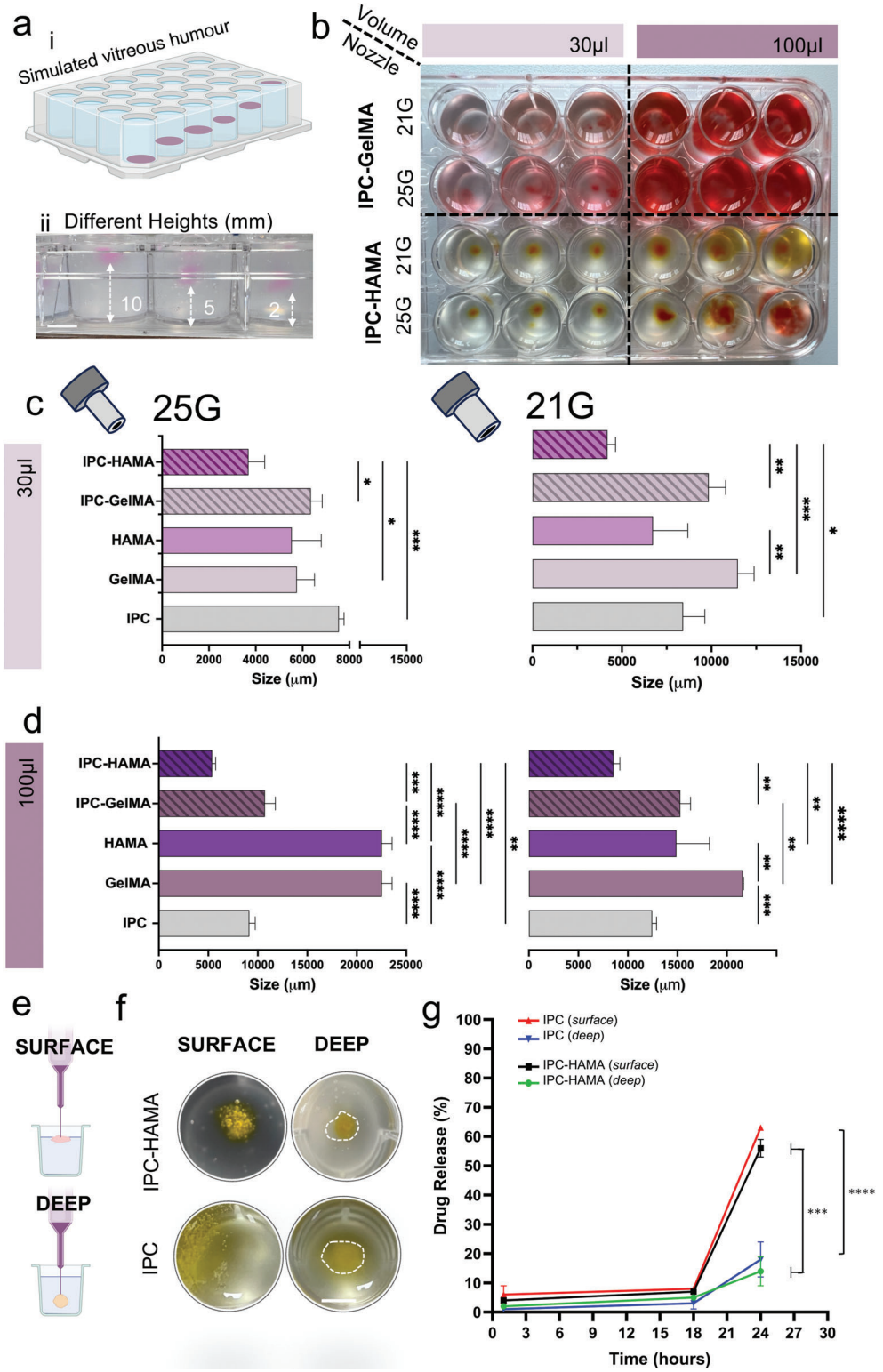

Figure 9. Deposition of IPC-based biomaterials using 3D printer for localized therapy. a) Bioprinting set-up in simulated vitreous humors at variable heights (2, 5 and 10 mm from the bottom of the well plate). b) 24-well plate demonstrate the dye diffusion test for IPC-HAMA and IPC-GelMA at different nozzle sizes and deposition volumes, c) dye released from micro-injected IPC-GelMA and IPC-HAMA at 30 µL and d) 100 µL for 25 and 21 G, respectively. e) Superficial and deep injection of IPC-composites to surface and deep locations in the support bath. f) Deep deposition of IPC-biomaterials using 3D printer resulted in improved scaffold formation. Mean ± SD, n = 3, **** $p < 0.0001$. Scale bars: 3 mm, g) The initial burst release profile of IgG from collagen-based composites injected at different depths within a 24-well plate. Mean values ± SD (n = 3), **** $p < 0.0001$ and *** $p < 0.001$.

Ethylenediaminetetraacetic acid (EDTA) disodium salt dihydrate (cat no. ED2SS), D-mannitol (cat no. M9546, MW: 182.17), Sodium bicarbonate (NaCHCO3, cat no. 13418), Sucrose (cat no. S7903), Sodium hydroxide (NaOH, 1 M, cat no. L1980), MES monohydrate (≥99.0%, cat no.69893), Sodium chloride (NaCl, ≥99.5%, cat no.S9888), 2-aminoethyl methacrylate hydrochloride (AEMA, 90%, cat no.516155), N-hydroxysuccinimide (NHS, 99%, cat no.56485), 1-[3-(Dimethylamino)-propyl]- 3-ethylcarbodiimide methiodide (EDC) (cat no.03450), Ru – Tris(2,2'-bipyridyl) dichloro-ruthenium (II) hexahydrate (cat no. 224758), Sodium persulfate (SPS) (cat no. 216232), Sodium phosphate monobasic monohydrate (MW:139.9, cat.no.567545), Gelatin – type A porcine skin (≈300 g bloom) (cat no. G1890), Methacrylic anhydride (cat no. 276685), Dulbecco's phosphate buffered saline (DPBS) (cat no. D8537), Ruthenium photoinitiator kit (cat no. 916811), Sodium Persulfate (cat no. 216232), Collagenase type I (cat no. SCR103), Collagen Assay Kit (cat. MAK322) and Agarose (cat. YA34896), Deuterium oxide (cat no. 320710075) was all purchased from sigma Aldrich. Spectrum Labs Spectra/Por 2 and 4 12–14 kD MWCO Standard RC Dry Dialysis Kits (cat no. 15390762), NHS-Rhodamine (cat no.46406), Dimethylsulfoxide (DMSO; cat no. 20688), Slide-A-Lyzer Dialysis Cassette, 10K MWCO (cat no.66380), Invitrogen NuPAGE 4 to 12%, Bis-Tris (cat no. 10338442), Thermo Scientific Pierce Silver Stain Kit (cat no. 10096113), Gibco Collagenase, Type I, powder (cat no.10114532) and Abnova Hyaluronidase (Bovine) (cat no. 16181770) all were purchased from Fisher Scientific. Hyaluronic acid sodium salt (Low molecular weight 40 – 50 kDa, cat no. FH01773) all were purchased from Biosynth. ORENCIA (abatacept, 250 mg), RoActemra (tocilizumab, 200 mg/10 mL) were provided from Moorfield eye hospital.

Synthesis of In Situ Polymerized Collagen: An in situ polymerizable collagen (IPC) was synthesized following a protocol described in a published patent[17,18] and further optimized in this study. Briefly, soluble type I collagen (15.0 mL, 6 mg mL^{-1}) was precipitated with NaCl (35.0 mL, 0.8 M). The tubes were gently shaken to flocculate the collagen in the solution before being centrifuged at high speed (4600 RPM) for 30 min at 4 °C. The white collagen precipitate collected at the bottom of each tube was carefully removed, and the excess supernatant was slowly squeezed out. The collected collagen was inserted into the washed dialyzed membrane (MWCO: 12–14 kDa, 10.0 cm in length), and both ends of the membrane were tied by dialysis tubing closures. The solution was then dialyzed against 0.1 M acetic acid to remove residual salts for 24 h. Following the initial dialysis, the collagen solution was then subjected to a second dialysis against 35 mM EDTA at a starting pH of 5.0 ± 0.2 for 24 h. The pH of the collagen solution was gradually increased from pH 5.0 to pH 7.0 during stepwise dialysis over 5 days. During the last step of dialysis, the collagen solution was dialyzed with 35 mM EDTA, 100 mM sucrose and 3.5% of D-mannitol.

To determine the concentration of the prepared IPC, a hydroxyproline assay was performed in accordance with the collagen kit manufacturer's protocol.[51] The collagen assay was initiated with enzymatic digestion, cleaving the protein into smaller peptides. Briefly, a serial dilution of a collagen type I standard was prepared (100 µL, 50 to 15 µg mL^{-1}). A master reaction solution was prepared by mixing digestive enzyme (0.5 µL) with a buffer solution (35.0 µL). Standard and IPC samples (20 µL) were transferred into a black, flat-bottom 96-well plate. The master reaction solution (30.0 µL) was then added to each well, and the plate was incubated at 37 °C for 60 min. Following incubation, a dye reagent (40 µL) was added to each well, and the plate was incubated for an additional 10 min. Finally, a developer (8 µL) was added to all wells, followed by a final 10-min incubation. Fluorescence intensity was measured at an excitation wavelength of 375 nm and an emission wavelength of 465 nm using a fluorometer plate reader (BMG FLUOstar Omega, Germany).

Synthesis of Methacrylated Hyaluronic Acid and Methacryloyl Gelatin: HAMA polymer was prepared by coupling the primary amine group of EDC/NHS with the carboxylic acid (ACOOH) group of HA (MW: 30 000–40 000) according to previously published protocols.[52,53] Briefly, 2% (w/v) HA was dissolved in a 0.05 M MES buffer solution (pH 6.5, 100 mL) containing NaCl (0.5 M). Then, the HA carboxylic acid groups were activated by adding NHS (46 mM) and EDC (59 mM) to the solution. After being completely dissolved, AEMA (0.76 g) was added dropwise to the mixture and stirred at room temperature for 24 h. The cross-linked HAMA was washed with acetone and dialyzed (MWCO = 3.5 kDa) against deionized water for 3 days. The final products were the lyophilized and stored at 4 °C.

In the second method, GelMA synthesis was carried out following a previously reported protocol.[54,55] Briefly, 10% (w/v) gelatin (type A3, ≈300 Bloom from porcine skin) was dissolved in PBS (10%, pH 7.5 ± 0.5) at 50 °C. Methacrylic anhydride (MA, 0.8 mL g^{-1}) was then added to the gelatin solution dropwise under vigorous stirring (≈500 RPM), and the mixture was allowed to react for 3 h at 50 °C in chemical safety fume hood. To eliminate toxic by-products, the resulting GelMA solution was dialyzed against deionized water using 1–2 kDa cut-off dialysis tubes for ≈5 days while the temperature was maintained at 50 °C. Finally, GelMA was lyophilized and kept at 4 °C for further use.

IPC-HAMA and IPC-GelMA Biomaterials: The biomaterials were prepared by dissolving either hyaluronic acid methacrylate (HAMA) or gelatin methacrylate (GelMA) (2% w/v) in 0.5 mL of deionized water (dH2O) under constant stirring at 40 °C for 1–2 h. The solutions were then transferred to black Eppendorf tubes to avoid light exposure. Sodium persulfate (SPS) (10 mM) and tris(2,2-bipyridyl) dichlororuthenium (II) hexahydrate (Ru) (1 mM, 10 µL) were added as photoinitiators, followed by thorough mixing using a vortex mixer. Next, the biomaterials were aspirated into 3 mL syringes with Luer-lock tips. These syringes were covered with aluminium foil to prevent light exposure during handling. A separate syringe was filled with IPC (250 µL, 23.7 mg mL^{-1}), maintaining a ratio of 1:2 to the HAMA or GelMA solution. The IPC gel and HAMA (or GelMA) were mixed using a syringe-to-syringe mixing method in a dark conditions to avoid light-induced reactions.

To study the biomechanical properties of IPC-blends biomaterials prior to 3D printing, poly (dimethyl siloxane) (PDMS, 5 mm diameter) molds were used. The biomaterials were then exposed to visible light (405 nm) for 10 min to induce photo-crosslinking. Finally, the cross-linked biomaterials were carefully removed from the molds and transferred to a 96-well plate containing PBS buffer (pH 7.4, 100 mM) for collagen fibrilization.

Preparation of Support Bath: Biomaterials were deposited using a 3D printer into a specialized support bath. Two support baths were prepared: (1) Agarose 0.5% w/v and (2) Agarose 0.2% w/v mixed with the HA (MW: 40–50 kDA, 0.15% w/v) to mimic the viscosity of the vitreous humor, which were used as simulated vitreous. Briefly, a 0.5% w/v solution of agarose was heated in an autoclave at 121 °C. The solution was then cooled with constant stirring to ensure even particle distribution as previously reported.[56]

The HA-Agar support bath was prepared by slowly adding 0.2% (w/v) agarose to PBS solution with a pH of 7.4 (100 mM) while stirring on a magnetic stirrer at 600 rpm for 10 min.[57] To solubilize the agarose in a hot buffer solution, the suspension was exposed for at least 20 min to saturated steam at 121 °C using an autoclave. The bottle containing the solution was allowed to slowly cool down in the autoclave at least 1 h to reach 80 °C. Hyaluronic acid (0.15%) was then immediately added to the suspension, followed by stirring at 700 rpm at room temperature for 24 h.

Swelling Ratio and Degradation Test: The swelling ratio and enzymatic degradation tests were performed on IPC biomaterials, following previously employed protocols.[58] To measure the swelling, gel samples were immersed in the PBS buffer solution and incubated at 37 °C. The blotting meshes were dried and weighed immediately after crosslinking and recorded as $m_{intial,dry}$. The swollen weight ($m_{swollen}$) was then recorded after 1 day. The swelling ratio (SR), was calculated using the following equation:

$$\text{Swelling ratio} = \frac{m_{swollen} - m_{initial,\,dry}}{m_{initial,dry}} \times 100\% \quad (1)$$

To conduct the degradation test on the IPC-based biomaterials, collagenase type-I was dissolved in a solution containing αMEM and $CaCl_2$ (0.3 M). Two concentrations were used for collagenase (0.1 and 1 mg mL^{-1}) for the slow degradation and fast degradation tests, respectively. The IPC-based biomaterials, with an average initial scaffold weight of ≈0.6 g, were

removed, dried, and weighed every 24 h. The percentage of degradation was calculated by the following formula:[59]

$$D = \frac{W_{0-}W_1}{W_0} \times 100\% \quad (2)$$

where W_0 was initial weight of the samples and W_1 is the weight at predetermined time points of the IPC samples and D is the percentage of degradation.

Rheological Testing: Rheological characterization of IPC, IPC-GelMA, and IPC-HAMA biomaterials was carried out using an MCR102 rheometer (Anton Paar, Austria) with a stepped Peltier plate. The temperature and time were controlled using a plate setup with a stainless-steel cone (plate diameter = 24.964 mm, cone angle = 2 degrees, truncation = 104 µm). An evaporation control system and an isolation hood were used to prevent solvent evaporation and sample drying. Flow curves were measured at T = 25 and 37 °C in the shear rate range $\gamma^{\cdot}$= (0.1–1000) s^{-1}. A pre-shear of $\gamma^{\cdot}$= 500 s^{-1} for 30 s, followed by a rest of 300 s before each measurement to erase any mechanical history. The amplitude sweeps with the frequency of 26 discrete steps were represented in a diagram with shear stress plotted on the x-axis and the storage modulus G′ and loss modulus G″ plotted on the y-axis by maintaining a 1% strain over a range from 0 to 100 Hz. Creep recovery measurements tests monitoring the storage, G′, and Loss, G″, moduli were also performed on Agarose and Agarose HA in oscillatory configuration at angular frequency $\omega = 6.28$ rad s^{-1}, during which immediate steps in deformation $\gamma = 1\%$ and $\gamma = 200\%$ were applied for almost 150 s followed by an interval at rest ($\gamma = 0$).

FTIR and ^{1}H-NMR Analysis: Fourier Transform Infrared (FTIR) spectrum of the individual components was examined on an Alpha FTIR Spectrometer (Bruker Optics, New Zealand) in order to evaluate the methacrylation of HAMA and GelMA. The freeze-dried samples were placed directly onto the ATR crystal, and FTIR spectra were obtained in the wavenumber range of 500 – 4000 cm^{-1} at 4 cm^{-1} resolution. Proton nuclear magnetic resonance (^{1}H-NMR) (Bruker Avance Neo) operating at 600 MHz was used to investigate the purity and degree of methacrylation of HAMA and GelMA.[60] ^{1}H-NMR samples were prepared by dissolving 2% (v/w) of HAMA or GelMa in deuterium oxide (D2O). The solutions were transferred to 5-mm ^{1}H-NMR glass tubes and spectra were obtained without allowing it to solidify completely.

SEM Imaging: The morphology and structure of molded specimens and 3D printed scaffolds were visualized by environmental scanning electron microscopy (SEM). Three solutions of IPC, IPC-HAMA, and IPC-GelMA were prepared and fibrilized by adding PBS buffer (pH 7.4) at 37 °C. The meshes were then mounted on a gold grid for analysis by environmental SEM.

Printing Parameters: The 3D printed cylinder construct was designed using computer-aided design (CAD) and Repetier-Host slicer software. In this study, two types of 3D bioprinters (3DBPs) were used to ensure reproducibility in the evaluation of the properties of IPC biomaterials. A custom-made 3DBP,[61] was employed for the dye dispersion tests, while a commercially available (BioX CellInk) 3DBP was utilized to fabricate composite hydrogel scaffolds for the drug release study. To generate continuous filaments of the different material inks, the printing parameters were adjusted to produce cylinders with a diameter of up to 10 mm and layer height of 3 mm. The syringe tip had an inner diameter of 250 µm, with a flow rate of 15–17 µL min^{-1} and print head speed of 160 mm min^{-1}. Finally, the printed cylinder was cured by exposing it to visible light at the wavelength of 405 nm for 10 min.

Drug Release Study in HA-Agar Support Bath: IgG antibody (tocilizumab, MW 150 kDa) was first labelled with the amine-reactive fluorescence dye, NHS-Rhodamine (MW of 528 Da), following the protocol.[62,63] The labelled IgG was then lyophilized using a freeze-drier, and the stability of lyophilized powder was studied using SDS-PAGE and Size-exclusion Chromatography (SEC). For the drug release study, the labelled IgG (2 mg) was mixed with biomaterials, followed by adding SPS (10 mM) and Ru (1 mM). The mixture was loaded into a 3D bioprinter (BioXCell). Two biomaterials were used for the comparison: IPC alone as a control and IPC-HAMA.

A cylindrical scaffold construct with specific dimensions (3 mm × 10 mm) and deposition volume (80 µL) was selected. After printing, the scaffolds were fibrilized and photo-crossed-linked. A sink condition was established by transferring the scaffolds into PBS buffer (1.0 mL, pH 7.0). Samples (1.0 mL) were collected for a duration of 82 days and replaced with 1.0 mL of PBS buffer. The fluorescence intensity of released IgG was measured at an excitation wavelength of 544 nm and an emission wavelength of 590 nm using a microplate reader.

To investigate IgG release in the context of enzymatic degradation and to evaluate the biodegradability of 3D-printed collagen-based scaffolds, a separate set of scaffolds was placed in a solution containing collagenase (0.5 mg mL^{-1}) and hyaluronidase (0.3 U mL^{-1}). The solution was refreshed daily with 1.0 mL of fresh enzyme solution, and the released IgG was measured until the scaffolds were completely degraded. The stability of the released IgGs was also analyzed using SDS-PAGE and silver staining techniques.

Images of collagen-based scaffolds undergoing enzymatic degradation were taken at intervals during a degradation study, specifically on random days within the experiment timeline. A Nikon SMZ18 microscope equipped for epifluorescence was used to take the images, utilizing specific filter sets: rhodamine (TAMRA, BODIPY-TMR analogues), GFP/Em: 580/(±) 60 (PyMPO). For experiments that examined the distribution of labelled IgG with fluorescent probes, a 300× objective was used, and the microscope settings, including fluorescence intensity and exposure at 25% and 300 ms time, were applied for each scaffold.

Dye Dispersion Studies in HA-Agar Support Bath: The HA-Agar support bath was transferred in a 12-well plate and placed on the print bed. Rhodamine dye was mixed with IPC-based biomaterials and loaded into the syringes. Two different sizes of syringes, 21 and 25 G were used. Two volume sizes, 30 and 100 µL of bioinks, were deposited within the support bath using the 3D bioprinter. The printed structures were exposed to visible light (405 nm) and the dyes were allowed to migrate for 30 min. The progression of rhodamine dyes was imaged and measured before and after fibrilization with a stereomicroscope (Zeiss) and diffusion was investigated using ImageJ software.

Localised Drug Delivery Using 3D Printer: A biologic (2.0 mg), a Fc-fusion protein with a structure similar to aflibercept (an anti-VEGF Fc-fusion protein approved for the treatment of AMD), was mixed with different biomaterials (1.0 mL each) of IPC alone, IPC-HAMA and IPC-GelMA. The drug-biomaterial mixtures (50 µL) were loaded into a syringe of a 3D-bioprinter and deposited into two different locations within 12-well plates: the surface and a deeper location within the HA-agar support bath. Photocrosslinking of the deposited biomaterials was achieved using visible light (405 nm) for 10 min. After crosslinking, 1.0 mL of PBS buffer (pH 7.4) was added to each well. The plates were then incubated at 37 °C to promote fibrilization. To study drug release, the buffer solution containing the released drug (1.0 mL) was removed from each well at specific time points (1, 18, and 24 h) and replaced with fresh PBS buffer (1.0 mL). The concentration of released biologic was measured using size exclusion bioHPLC column (Agilent Zorbax GF-250, USA) with an Agilent Infinity II HPLC system (Agilent, Waldbronn, Germany).

Statistical Analysis: All experiments were performed in $n \geq 3$ and were presented as the mean ± standard deviation (SD). Statistical differences were evaluated using one way ANOVA test with post-hoc Tukey's test. The significance was also determined as a *p*-value (< 0.05) using Prism 10.0.0 (GraphPad Holdings, San Diego, CA, USA).

Supporting Information

Supporting Information is available from the Wiley Online Library or from the author.

Acknowledgements

H.K. is grateful for the funds from the Royal Society, Research Grant. H.H.K is Ph.D. student at UWL who is grateful for the Vice-Chancellor Scholarship

to support his PhD studies. RA acknowledges financial support from European Union – Next Generation EU, Project PRIN 2022ZA77J2 ICARUS, CUP B53D23009010006, National Recovery and Resilience Plan (NRRP) Mission 4, Component 2, Investment 1.1. This research was partially funded by grants from ERC-2019-Synergy Grant (ASTRA, n. 855923); EIC-2022-PathfinderOpen (ivBM-4PAP, n. 101098989); Project "National Center for Gene Therapy and Drugs based on RNA Technology" (CN00000041) financed by NextGeneration EU PNRR MUR—M4C2—Action 1.4—Call "Potenziamento strutture di ricerca e creazione di "campioni nazionali di R&S" (CUP J33C22001130001). Cartoons in figures were created with BioRender.

Conflict of Interest

The authors declare no conflict of interest.

Data Availability Statement

The data that support the findings of this study are available from the corresponding author upon reasonable request.

Keywords

3D Bioprinting, collagen, eye treatment, gelatin, hyaluronic acid

Received: June 27, 2024
Revised: October 20, 2024
Published online:

[1] D. Scuteri, A. Vero, M. Zito, M. D. Naturale, G. Bagetta, C. Nucci, P. Tonin, M. T. Corasaniti, *Neural Regener. Res.* **2019**, *14*, 1445.
[2] R. C. Cooper, H. Yang, *J. Controlled Release* **2019**, *306*, 29.
[3] R. Tarragó, J. L. Olea, C. Ramírez, L. Escudero, *Arch. Soc. Esp. Oftalmol.* **2017**, *92*, 107.
[4] M. Xu, R. Fan, X. Fan, Y. Shao, X. Li, *Drug Des. Dev. Ther.* **2022**, *16*, 3241.
[5] A. A. Al-Kinani, G. Zidan, N. Elsaid, A. Seyfoddin, A. W. G. Alani, R. G. Alany, *Adv. Drug Delivery Rev.* **2018**, *126*, 113.
[6] H. Khalili, H. H. Kashkoli, D. E. Weyland, S. Pirkalkhoran, W. R. Grabowska, *Pharmaceuticals (Basel)* **2023**, *16*, 620.
[7] D. S. Rajendran Nair, M. J. Seiler, K. H. Patel, V. Thomas, J. C. Martinez Camarillo, M. S. Humayun, B. B. Thomas, *Appl. Sci. (Basel)* **2021**, *11*, 2154.
[8] S. Liu, C.-S. Lau, K. Liang, F. Wen, S. H. Teoh, *Curr. Opin. Biotechnol.* **2022**, *74*, 92.
[9] R. Naomi, P. M. Ridzuan, H. Bahari, *Polymers (Basel)* **2021**, *13*, 2642.
[10] S. Yao, Y. Zhao, Y. Xu, B. Jin, M. Wang, C. Yu, Z. Guo, S. Jiang, R. Tang, X. Fang, S. Fan, *Adv. Healthcare Mater.* **2022**, *11*, e2200516.
[11] Z. An, J. Wu, S.-H. Li, S. Chen, F.-L. Lu, Z.-Y. Xu, H.-W. Sung, R.-K. Li, *Theranostics* **2021**, *11*, 3948.
[12] N. Raina, R. Pahwa, J. Bhattacharya, A. K. Paul, V. Nissapatorn, L. de, M. Pereira, S. M. R. Oliveira, K. G. Dolma, M. Rahmatullah, P. Wilairatana, M. Gupta, *Pharmaceutics* **2022**, *14*, 574.
[13] T. Vermonden, R. Censi, *Chem. Rev.* **2012**, *112*, 2853.
[14] V. Delplace, A. Ortin-Martinez, E. L. S. Tsai, A. N. Amin, V. Wallace, M. S. Shoichet, *J. Controlled Release* **2019**, *293*, 10.
[15] T. R. Hoare, D. S. Kohane, *Polymer (Guildf)* **2008**, *49*, 1993.
[16] D. M. Darvish, *Mater. Today Bio* **2022**, *15*, 100322.
[17] D. Devore, J. Zhu, R. Brooks, R. R. McCrate, D. A. Grant, S. A. Grant, *J. Biomed. Mater. Res. Part A* **2016**, *104*, 758.
[18] D. Devore, R. Brooks, T. Byrnes, US10111981B2 **2014**.
[19] R. Dimatteo, N. J. Darling, T. Segura, *Adv. Drug Delivery Rev.* **2018**, *127*, 167.
[20] F. Xu, C. Dawson, M. Lamb, E. Mueller, E. Stefanek, M. Akbari, T. Hoare, *Front. Bioeng. Biotechnol.* **2022**, *10*, 849831.
[21] Y. Zhang, Y. Wang, Y. Li, Y. Yang, M. Jin, X. Lin, Z. Zhuang, K. Guo, T. Zhang, W. Tan, *Gels* **2023**, *9*, 185.
[22] Y.-H. Jiang, Y.-Y. Lou, T.-H. Li, B.-Z. Liu, K. Chen, D. Zhang, T. Li, *Am. J. Transl. Res.* **2022**, *14*, 1146.
[23] R. Varela-Fernández, V. Díaz-Tomé, A. Luaces-Rodríguez, A. Conde-Penedo, X. García-Otero, A. Luzardo-Álvarez, A. Fernández-Ferreiro, F. Otero-Espinar, *Pharmaceutics* **2020**, *12*, 269.
[24] E. Dosmar, J. Walsh, M. Doyel, K. Bussett, A. Oladipupo, S. Amer, K. Goebel, *Bioengineering (Basel)* **2022**, *9*, 41.
[25] Q. Xu, J. E. Torres, M. Hakim, P. M. Babiak, P. Pal, C. M. Battistoni, M. Nguyen, A. Panitch, L. Solorio, J. C. Liu, *Mater. Sci. Eng.: R. Rep.* **2021**, *146*, 100641.
[26] L. I. Los, R. J. van der Worp, M. J. A. van Luyn, J. M. M. Hooymans, *Invest. Ophthalmol. Visual Sci.* **2003**, *44*, 2828.
[27] P. N. Bishop, *Prog. Retinal Eye Res.* **2000**, *19*, 323.
[28] N. K. Tram, K. E. Swindle-Reilly, *Front. Bioeng. Biotechnol.* **2018**, *6*, 199.
[29] Z. Gu, J. Fu, H. Lin, Y. He, *Asian J Pharm. Sci.* **2020**, *15*, 529.
[30] G. Tan, N. Ioannou, E. Mathew, A. D. Tagalakis, D. A. Lamprou, C. Yu-Wai-Man, *Int. J. Pharm.* **2022**, *625*, 122094.
[31] A. Samadi, A. Moammeri, M. Pourmadadi, P. Abbasi, Z. Hosseinpour, A. Farokh, A. Shamsabadipour, M. Heydari, M. R. Mohammadi, *ACS Biomater. Sci. Eng.* **2023**, *9*, 1862.
[32] S. Khunmanee, Y. Jeong, H. Park, *J. Tissue Eng.* **2017**, *8*, 204173141772646.
[33] S. Santhanam, J. Liang, R. Baid, N. Ravi, *J. Biomed. Mater. Res. Part A.* **2015**, *103*, 2300.
[34] N. Nakajima, Y. Ikada, *Bioconjugate Chem.* **1995**, *6*, 123.
[35] P. Bulpitt, D. Aeschlimann, *J. Biomed. Mater. Res.* **1999**, *47*, 152.
[36] M. D'Este, D. Eglin, M. Alini, *Carbohydr. Polym.* **2014**, *108*, 239.
[37] B. H. Lee, H. Shirahama, N.-J. Cho, L. P. Tan, *RSC Adv.* **2015**, *5*, 106094.
[38] A. Gulzar, E. Yildiz, H. N. Kaleli, M. A. Nazeer, N. Zibandeh, A. N. Malik, A. Y. Tas, I. Lazoglu, A. Sahin, S. Kizilel, *Acta Biomater.* **2022**, *147*, 198.
[39] D. A. Fancy, T. Kodadek, *Proc. Natl. Acad. Sci. USA* **1999**, *96*, 6020.
[40] J. W. Bjork, S. L. Johnson, R. T. Tranquillo, *Biomaterials* **2011**, *32*, 2479.
[41] Q. Zhang, K. Yan, X. Zheng, Q. Liu, Y. Han, Z. Liu, *Mater. Today Bio* **2024**, *26*, 101082.
[42] K. S. Lim, B. J. Klotz, G. C. J. Lindberg, F. P. W. Melchels, G. J. Hooper, J. Malda, D. Gawlitta, T. B. F. Woodfield, *Macromol. Biosci.* **2019**, *19*, 1900098.
[43] K. N. Bitar, E. Zakhem, *Biomed. Eng. Comput. Biol.* **2014**, *6*, BECBS10961.
[44] B. P. Chan, K. W. Leong, *Eur. Spine J.* **2008**, *17*, 467.
[45] G. Cidonio, C. R. Alcala-Orozco, K. S. Lim, M. Glinka, I. Mutreja, Y.-H. Kim, T. B. F. Woodfield, R. O. C. Oreffo, *Biofabrication* **2019**, *11*, 035027.
[46] D. J. Oshannessy, R. H. Quarles, *J. Immunol. Methods* **1987**, *99*, 153.
[47] C. Cilliers, I. Nessler, N. Christodolu, G. M. Thurber, *Mol. Pharmacol.* **2017**, *14*, 1623.
[48] M. Murata, A. Kawamura Jr., *Microbiol. Immunol.* **1980**, *24*, 65.
[49] B. A. Filas, Q. Zhang, R. J. Okamoto, Y. B. Shui, D. C. Beebe, *Invest. Ophthalmol. Visual Sci.* **2014**, *55*, 55.
[50] M. Hammer, M. Muuss, S. Schickhardt, A. Scheuerle, R. Khoramnia, G. Łabuz, P. Uhl, G. U. Auffarth, *Invest. Ophthalmol. Visual Sci.* **2024**, *65*, 36.

[51] Sigma-Aldrich. Collagen Assay Kit [Internet], Sigmaaldrich.com, [cited 2024 May 21]. https://www.sigmaaldrich.com/deepweb/assets/sigmaaldrich/product/documents/223/444/mak322bul.pdf.
[52] A. Laezza, A. Pepe, B. Bochicchio, *Chemistry* **2022**, *28*, e202201959.
[53] K. A. Smeds, M. W. Grinstaff, *J. Biomed. Mater. Res.* **2001**, *54*, 115.
[54] M. Costantini, J. Idaszek, K. Szöke, J. Jaroszewicz, M. Dentini, A. Barbetta, J. E. Brinchmann, W. Święszkowski, *Biofabrication* **2016**, *8*, 035002.
[55] M. Sun, X. Sun, Z. Wang, S. Guo, G. Yu, H. Yang, *Polymers (Basel)* **2018**, *10*, 1290.
[56] G. Cidonio, M. Cooke, M. Glinka, J. I. Dawson, L. Grover, R. O. C. Oreffo, *Mater. Today Bio.* **2019**, *4*, 100028.
[57] T. Auel, L. P. Scherke, S. Hadlich, S. Mouchantat, M. Grimm, W. Weitschies, A. Seidlitz, *Pharmaceutics* **2023**, *15*, 786.
[58] K. Rahali, G. Ben Messaoud, C. Kahn, L. Sanchez-Gonzalez, M. Kaci, F. Cleymand, S. Fleutot, M. Linder, S. Desobry, *Int. J. Mol. Sci.* **2017**, *18*, 2675.
[59] X. Zhao, Q. Lang, L. Yildirimer, Z. Y. Lin, W. Cui, N. Annabi, K. W. Ng, M. R. Dokmeci, A. M. Ghaemmaghami, A. Khademhosseini, *Adv. Healthcare Mater.* **2016**, *5*, 108.
[60] Y. Wang, L. H. Koole, C. Gao, D. Yang, L. Yang, C. Zhang, H. Li, *NPJ Regener. Med.* **2022**, *7*, 74.
[61] S. Mohammadi, S. D'Alessandro, F. Bini, F. Marinozzi, G. Cidonio, *HardwareX* **2023**, *18*, e00527.
[62] E. Harlow, D. Lane, *Antibodies; A Laboratory Manual*, Cold Spring Harbor Laboratory, New York **1988**.
[63] Thermofisher.com. [cited 2024 Jun 19], https://assets.thermofisher.com/TFS-Assets/LSG/manuals/MAN0011648_NHSRhodamine_UG

